NASA TECHNICAL NOTE

NASA TN D-8079

4.

DEVELOPMENT OF AN AIRBORNE LASER BATHYMETER

Hongsuk H. Kim, Peter O. Cervenka, and Charles B. Lankford

Wallops Flight Center
Wallops Island, Va. 23337

3.
NATIONAL AERONAUTICS AND SPACE ADMINISTRATION • WASHINGTON, D. C. • OCTOBER 1975

5.

1. Report No.	2. Government Accession No.	3. Recipient's Catalog No.
NASA TN D-8079		

4. Title and Subtitle	5. Report Date
DEVELOPMENT OF AN AIRBORNE LASER BATHYMETER	October 1975
	6. Performing Organization Code

7. Author(s)	8. Performing Organization Report No.
Hongsuk H. Kim (NASA Wallops Flight Center) Peter O. Cervenka and Charles B. Lankford (Computer Sciences Corporation)	
	10. Work Unit No.
9. Performing Organization Name and Address	
NASA Wallops Flight Center, Wallops Island, Virginia 23337 Computer Sciences Corporation, Wallops Island, Virginia 23337	11. Contract or Grant No.
	13. Type of Report and Period Covered
12. Sponsoring Agency Name and Address	TECHNICAL NOTE
National Aeronautics and Space Administration Washington, DC 20546	14. Sponsoring Agency Code

15. Supplementary Notes

16. Abstract

An airborne laser depth sounding system has been built and taken through a complete series of field tests. Two green laser sources have been tried: a pulsed neon laser at 540 nm and a frequency-doubled Nd:YAG transmitter at 532 nm. To obtain a depth resolution of better than 20 cm, the pulses had a duration of 5 to 7 nanoseconds and could be fired up to at rates of 50 pulses per second. In the receiver, the signal was detected by a photomultiplier tube connected to a 28 cm diameter Cassegrainian telescope that was aimed vertically downward.

Oscilloscopic traces of the signal reflected from the sea surface and the ocean floor could either be recorded by a movie camera on 35 mm film or digitized into 500 discrete channels of information and stored on magnetic tape, from which depth information could be extracted. An aerial color movie camera recorded the geographic footprint while a boat crew of oceanographers measured depth and other relevant water parameters.

About two hundred hours of flight time on the NASA C-54 airplane in the area of Chincoteaque, Virginia, the Chesapeake Bay and in Key West, Florida, have yielded information on the actual operating conditions of such a system and helped to optimize the design. One can predict the maximum depth attainable in a mission by measuring the effective attenuation coefficient in flight. This quantity is four times smaller than the usual narrow beam attenuation coefficient.

Several square miles of a varied underwater landscape have also been mapped. Such a system can be either used alone in a scanning device or in conjunction with aerial photography to serve as reference. In either case, it promises great savings in time and expense over the usual sounding techniques.

17. Key Words (Suggested by Author(s))	18. Distribution Statement
Airborne Laser Bathymeter Hydrographic Chart Space-Oceanography Laser Applications	Unclassified - Unlimited STAR Category 48

19. Security Classif. (of this report)	20. Security Classif. (of this page)	21. No. of Pages	22. Price*
Unclassified	Unclassified	39	$3.75

*For sale by the National Technical Information Service, Springfield, Virginia 22161

DEVELOPMENT OF AN AIRBORNE LASER BATHYMETER

by

Hongsuk H. Kim
NASA Wallops Flight Center

and

Peter O. Cervenka
Charles B. Lankford
Computer Sciences Corporation

INTRODUCTION

The idea of ranging underwater with a pulsed laser was first proposed in the late sixties.[1] In 1968, G. D. Hickman of Syracuse University Research Corporation was the first to demonstrate such a system in flight.[2] The Naval Oceanographic Office in Washington, DC conducted a series of field tests with their first breadboard model known as Pulsed Light Airborne Depth Sounder (PLADS) between 1971 and 1972.[3] However in either case, the results of the field experiments were not sufficient to guarantee either the performance of such a technique for sustained field missions, or its cost effectiveness in comparison with other available means of depth sounding.

The capability of an Airborne Laser Bathymeter (ALB) System to perform hydrographic surveys quickly from an aircraft at speeds of hundreds of knots has become a matter of considerable interest for military amphibious troop landing and peace time geological survey. In December 1973, the NASA Wallops Flight Center lidar research group and the U.S. Naval Oceanographic Office agreed upon a joint program to develop and evaluate the technique with the ultimate goal of constructing "a more reliable and complete" operational ALB unit in the near future (Appendix A). In this agreement, NASA's group, with its experience in airborne laser fluorosensing, was to be responsible for hardware development and field testing; while the Naval group would provide requirements and available information on the PLADS project. The work was initiated in December 1973 and completed in March 1975. This technical note compiles the results of our 15-month period of developmental and test effort.

THEORY

Conventional laser ranging systems, such as the laser geodolite, extract information from the phase delay at the modulation frequency between the light emitted and received. The laser beam from an airborne platform undergoes several orders of magnitude attenuations as it propagates through water. This dictates the use of high peak powers which are only practically available in lasers having low repetition rates.

Airborne laser bathymetry hinges on the simple idea of sending vertically downward a light pulse having a duration of a few nanoseconds. The time delay between the light pulse reflected from the water surface and the one coming from the ocean floor yields water depth information (fig. 1). The usefulness of the method depends totally on the interaction of several unpredictable factors which affect water turbidity and bottom reflectance.

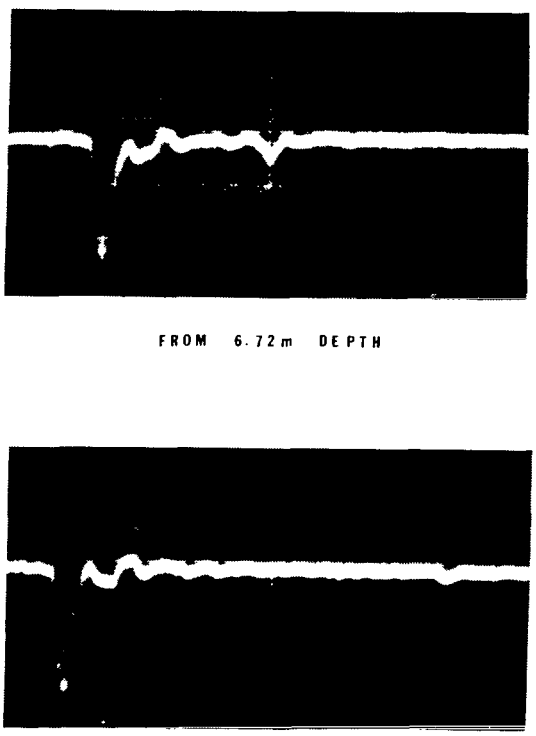

Figure 1. - Oscilloscopic traces of laser returns.

The theoretical analysis included in this study must, of necessity, only deal with the fundamental aspects of the problem. Additional material has been included only when it has a direct bearing on the interpretation of the field data and the performance of an ALB system.

An airborne platform used to range a surface at a distance, H, sees a power, P(rec), coming back to it when the target spot size is small compared to the distance, H.

$$P(rec) = \frac{P(\ell)\ \rho \cdot e^{-2KH}\ (A \cdot E)}{2\pi\ H^2} \quad . \tag{1}$$

Here, $P(\ell)$ is the transmitted laser power and ρ is the surface reflectance. The last two factors, A and E, denote respectively the area and the efficiency of the detector and K is the atmospheric attenuation constant. If t is the elapsed time for the light pulse, then the distance covered H is

$$H = \frac{ct}{2} \tag{2}$$

where c is the speed of light.

On a clear day, visible light is not attenuated very much by several hundred meters of atmosphere. When ranging water depth, one first observes a strong light pulse returned by the water surface. The portion of the pulse that finally gets to the receiver after interacting with the ocean floor can be expressed as

$$P(rec) = \frac{P(\ell)\ R \cdot (1-\rho) e^{-2(KH + \gamma L)}}{2\pi\ (H + L)^2} \quad . \tag{3}$$

For a layer of water of depth, L, the above expression includes the effective attenuation coefficient, γ, as measured by the receiver.* The value of L is related to the time interval ΔT between the 2 pulses by

$$L = \frac{c\ T}{2\ n_{water}} \tag{4}$$

where n_{water} is the refractive index of water.

---

* An expression for the power coming back to the surface of a nonscattering medium within the receiver field of view is given in Appendix B.

Oceanographers with an interest in underwater imaging measure an attenuation coefficient, α, using a transmissometer. This instrument measures the amount of light through a highly collimated optical path of length, L. There are light losses due to the absorption, a, and scattering, s, and α is defined as the sum of contributions from both.

$$\alpha = a + s . \tag{5}$$

A typical light scattering arrangement is shown in figure 2. A lot of light scattered at $\theta° \neq 0$ by suspended particles would not be caught by the α-meter at P_1 but would still be within the field of view of the bathymeter. This geometry applies to an airborne detector since the latter sees a much larger area. (See the figure in Appendix B.) Hence, we would expect the ALB to measure an attenuation coefficient smaller than that given by the conventional method.

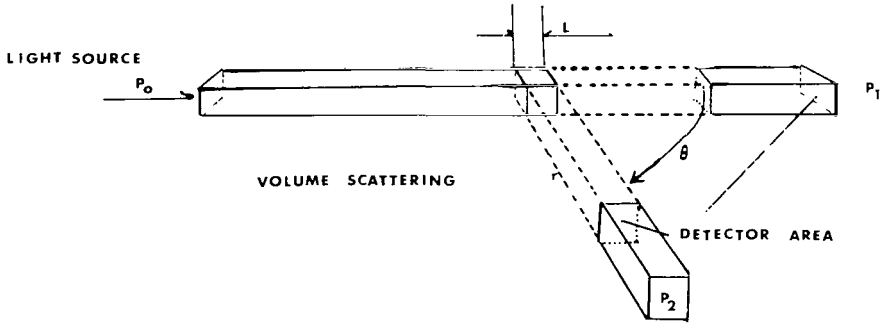

Figure 2. - Photometer geometry.

When one measures the light loss, dp, due to absorption by a length, L, in a non-scattering fluid, one can define an absorption cross section, $\sigma(a)$,

$$\frac{dp}{P_o} = \sigma(a) L . \tag{6}$$

Optical properties of sea water are greatly affected by the size distribution and index of refraction of the suspended particles it contains.

In 1963, S. Q. Duntley pointed out that the light distribution due to the scattering was highly peaked in the forward direction.[4] This fact was confirmed by others. G. D. Hickman showed that in the case of laser light, the beam intensity drops several orders of magnitude when measured between 1° and 90°.[5] A scattering cross section, $\sigma(\theta)$, per unit solid angle can be defined as

$$\frac{dp}{P_o} = \sigma(\theta) \frac{A}{r^2} . \tag{7}$$

This can be related to W. H. Wells' broad beam attenuation coefficient γ, by[6]

$$\gamma \equiv a + s\ (>10°) \tag{8}$$

where $$s\ (>10°) = \int_{1/6}^{\pi} \sigma(\theta)\ 2\pi \sin\ \theta d\theta \tag{9}$$

or $$\alpha \equiv a + s\ (<10°)$$

$$s\ (<10°) = \int_{0}^{1/6} \sigma(\theta)\ dw\ . \tag{10}$$

We can see that the broad beam attenuation coefficient of Wells is a more realistic parameter for our ALB application since it encompasses the contribution from scattered light that can still manage to enter the receiver.

INSTRUMENTATION

System Description

In December 1973, the PLADS system was transferred to NASA Wallops. A careful examination of the unit showed that the data processing section was faulty in design and the transmitter was totally inoperable. It would have required considerable time and effort to retrieve the unit; therefore, a decision was made not to repair the PLADS. Instead, NASA's airborne laser fluorosensing unit was modified for laser bathymetry. The NASA unit was originally designed to study laser induced fluorescence from various marine constituents and had been constructed to fit the NAS-427 aircraft.[7] The salient feature of the unit is a 28 cm diameter, f-1, Cassegrainian telescope which is mounted on a rigid aluminum channel structure as shown in figure 3. A large space to the right of the upright telescope, was originally used for mounting an AVCO C-950 pulsed gas (either nitrogen or neon) laser. The transmitter shown in the picture is a frequency doubled Nd:YAG system which occupies only 23 x 28 x 64 cm and weighs 18 kgs. The frame was made out of 5 x 10 cm aluminum beams rigidly welded together and shock mounted along the seat tracks on the floor of the DC aircraft. The short focal length of the primary mirror allowed the receiver assembly to be mounted upright and to point directly downward through the openings of the floor and outer skin of the aircraft. The total weight of the floor package was about 136 kgs with the Avco gas laser unit and about 90 kgs with the Nd:YAG laser unit.

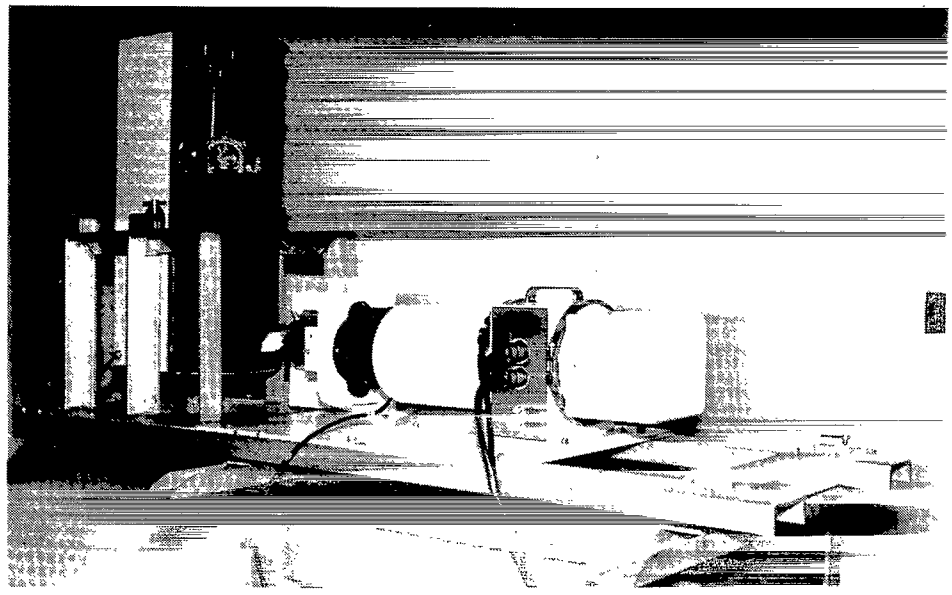

Figure 3. - NASA's ALB unit.

The NAS-427 aircraft is a military version of the DC-4. It is a four engine, low-wing monoplane with fully retractable tricycle landing gear. It is powered by four, 14 cylinder twin-row aircooled Pratt-Whitney R-2000 engines and can carry a cargo load of approximately 5400 kgs. The plane has been modified to carry active and passive remote sensing equipment with their control, power and data collecting systems mounted in a row of 48 cm racks. Table I summarizes the NASA-ALB units' components and the pertinent design parameters.

TABLE I. - COMPONENTS AND CHARACTERISTICS OF NASA'S ALB SYSTEM USED FOR THE JOINT NAVY-NASA TESTS

a) TRANSMITTERS:

Output Wavelength	540 nm (neon ion laser)	532 nm (frequency doubled Nd: YAG laser)
Peak Power	2KW	2MW
Pulse Duration	6nsec	8nsec
Rep Rate	10-200 pps	10-50 pps

b) RECEIVER:

28 cm Diameter Cassegrainian Telescope, f-1

PMT: 8575 RCA

Filter. 0.4 nm at FWHM at 540 nm, 532 nm

c) RECORDING DEVICES

Flight Research Movie Camera with 4X-Film

Waveform Digitizer (Modified Optical Multichannel Analyzer) and a 9-Track Mag Tape Recorder

d) AIRCRAFT USED:

C-54, Military Version of DC-4

Altitudes: 150 and 600 meters at 150 knots

Navigational Information: An aerial footprint camera (35 mm)

Transmitters Evaluated

For pulsed mode operation, only two lasers are commercially available and applicable to bathymetry. They are a pulsed neon ion laser (540 nm), and a frequency doubled Nd:YAG laser at 532 nm. A copper vapor laser held a promising outlook in its repetition rate and average power, but the laser was still in the development stage and not commercially available at the time of laser selection.

A blue-green dye laser which is optically pumped with a nitrogen ultraviolet laser was also strongly considered, but the 10 to 12 nanoseconds pulse duration was judged to be unsuitable for a depth resolution of 30 cm or less.

Therefore, in the earlier tests of December 1973 and August 1974 in Key West the existing Avco C-950 neon gas flow laser was used. Originally the unit had a nominal green color output of 35 microjoules in 5 nanoseconds. Later, the laser was fitted with an unstable resonant cavity composed of two Cassegrainian mirrors. With the modification, the physical divergence of the output beam was changed from 2 x 30 milliradians to 2 x 5 milliradians for the new system. A careful measurement of the peak power indicated no more than 12 microjoules in a 6 nanoseconds duration.

The Nd:YAG laser unit which was evaluated in the February 1975 flight tests is Pockels cell Q-switched, frequency doubled, and capable of providing a power output of 10 millijoules in 8 nanoseconds at a maximum repetition rate of 50 pps. The output beam divergence can be as narrow as 2 milliradians when used with beam-collimating optics. Transmitter cooling is via a closed cycle, self-contained system.

Receiver Assembly

As shown in figure 3, a 28 cm diameter, f-1, Cassegrainian telescope is the main feature. The return signals gathered by the telescope pass through two remote controlled filter wheels with six slots in each. One of the wheels contains six different grades of neutral density filters. The other wheel has six narrow band-pass filters. The filters have the band pass width of 4 angstroms at the half intensity points of the respective center wavelengths. An RCA 8575 photomultiplier tube was used. The output of the PM tube was terminated with a 50 ohm resistor.

Data Acquisition, Processing, and Recording

The block diagram of figure 4 shows the outlay of NASA's ALB system. The display and analysis of very fast, single shot pulses have long been one of the difficulties in instrumentation. Of concern to the bathymetric information are duration and amplitudes of two successive peaks of each waveform. Because the event occurs in the time window of two hundred nanoseconds, the input gate of the return signal from the PM tube was normally closed. The oscilloscopic sweep began only when a gating signal from an altitude delay compensated sync signal reached the scope's external trigger. Then the oscilloscopic display of individual shots was recorded using either of the following methods.

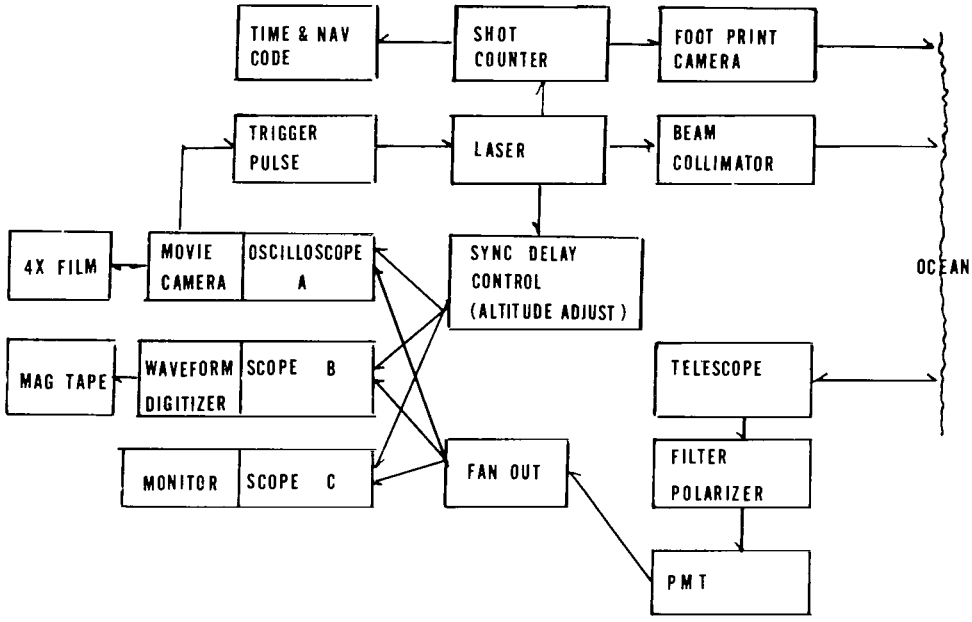

Figure 4. - Block diagram of NASA's ALB system.

Movie Camera. - One sure way to record fast transients has been to use a movie camera and record the oscilloscope trace. A 35 mm Flight Research movie camera, (Multidata Model IV-C) was used with a Tektronix 475 scope with P-11 phosphor. The camera was driven at 10 frames per second, thereby limiting the laser firing rate to 10 pps. Since the camera was free running, the laser had to be triggered by the camera. A stationary microswitch riding on a cam inside the camera drove two monostable multivibrators to

create noise free, very short laser trigger pulses. Lab studies have shown us that Eastman Kodak 4X negative 5224 film (ASA-1,000) was most suitable for the purpose. Many thousand frames of ALB return signals have been recorded in this manner. However, obvious disadvantages are: the time required to develop the photographic images, and each image requires manual viewing analysis.

On-Line Hardwired Device. - The most pertinent information in ALB is the time interval measurement of the two peaks. Even before the waveforms are being displayed on an oscilloscope, threshold triggering techniques could probably be working detecting the two crests. The data processing of the PLADS unit was based on this approach. A research and development grant was awarded to Dr. Trehan of Hampton Institute, Hampton, VA for the fabrication of a prototype time interval counter.* The package was delivered to NASA just prior to the August 1974 Key West flight test and could not be adapted into the system in time. However, the August test has shown us that a significant portion of the return data is of a marginally small amplitude and the threshold triggering technique would have had difficulty operating among the spurious noise spikes. Subsequent efforts were focused on the development of a total waveform digitizer of high repetition rate.

Quasi Two Dimensional Waveform Digitizer. - One company advertises a total waveform digitizer, including a minicomputer to perform real time analysis of transient pulse. Upon inspection, this system was found to have a maximum repetition rate of 5 frames per second, whereas we required a minimum of 10-30 pulses a second. This initiated extensive work to develop our own waveform digitizer. In our approach an optical multichannel analyzer (OMA) along with its fast analog to digital conversion capability was utilized. The OMA provides simultaneous detection of 500 segments of a dispersed light intensity focused on the target of a silicon vidicon. The photon intensity incident on each segment (or channel) is integrated, digitized and transferred to a digital tape recorder at the maximum rate of 30 scans per second. In order to compress an X-Y dimensional waveform from the oscilloscope screen into one dimensional streak on the silicon surface, an optical arrangement shown in figures 5 and 6 was devised. In figure 5, A is a masked device to obstruct baseline phosphorescence of the oscilloscope trace, B is a cylinderical lens, C is a focusing lens, and D is the imaged scope trace in one dimension. The trace imaged on the silicon target produces an intensity modulation which is roughly proportional to the amount of deflection on the original scope. Thus we were able to record 200 nsec traces in a digitized format at the repetition rate of 30 frames per second. A typical example of a digitized waveform from the unit is shown in figure 7.

---

* NGR-47-020-006

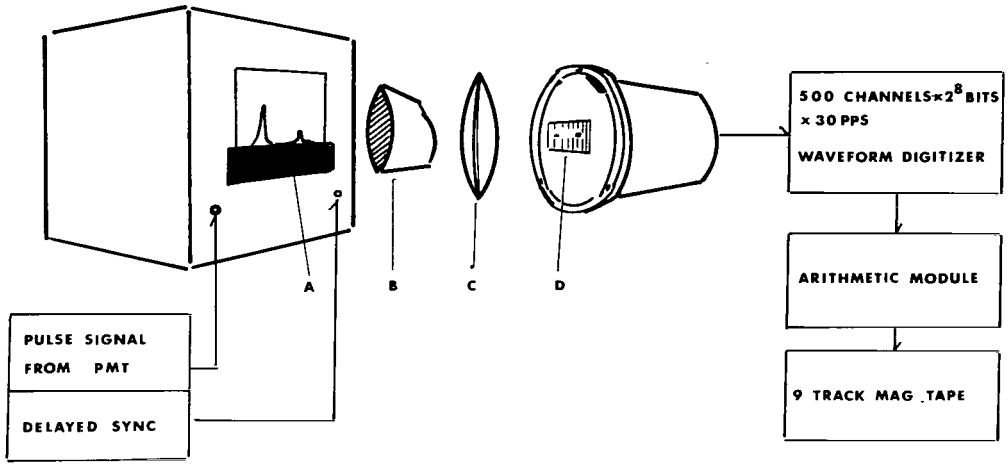

Figure 5. - Schematic diagram of the waveform digitizer.

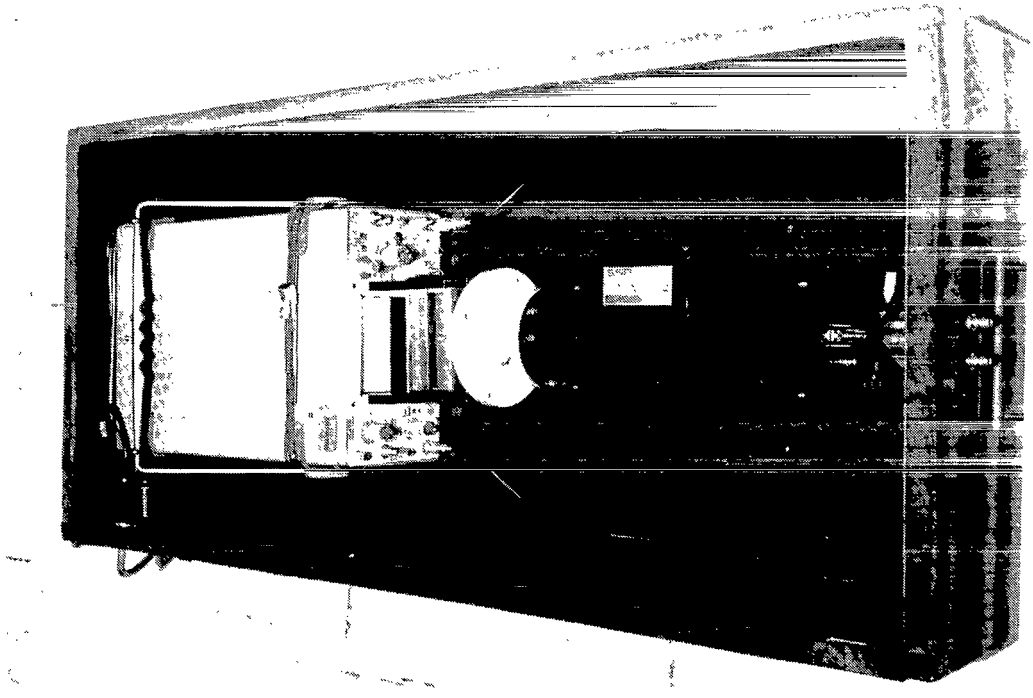

Figure 6. - Waveform digitizer.

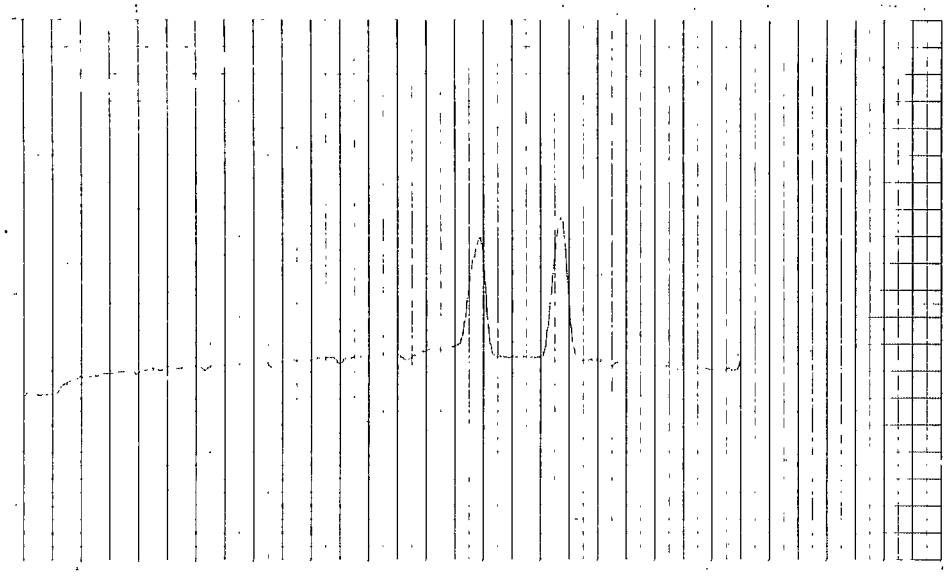

Figure 7. - Waveform digitizer printout.

FIELD TESTS

It was originally planned that the ALB would be flight tested by the NAS-427 aircraft off the coast of Chincoteague Island and in the Chesapeake Bay. However, flights in the early summer of 1974 in these areas showed that the water attenuation coefficient (α) of the optical beam ranged from 3.0 to 5.0 m^{-1}. The bottom reflectance was typically 5 to 7%. Under these conditions, it would be extremely difficult to detect any laser returns even from a 2-meter depth. Therefore, follow-on flights were planned for the area off the coast of Key West in the Gulf of Mexico.

Key West Flight Tests

For the Key West test, a flight plan was developed which provided for repeated flights of the ALB unit over a confined test area until all the ALB parameters became known against the known sea-truth of the area. Thus, a narrow strip of flight line was selected off Boca Chica Key as shown in figure 8 map in August 1974. The survey line stretching between Saddlebunch Key and Middle Sambo (through the C-55 Marker Buoy in Hawk Channel) contains several remnant coral heads, a deep channel and monotonously graded coarse sandy slopes.

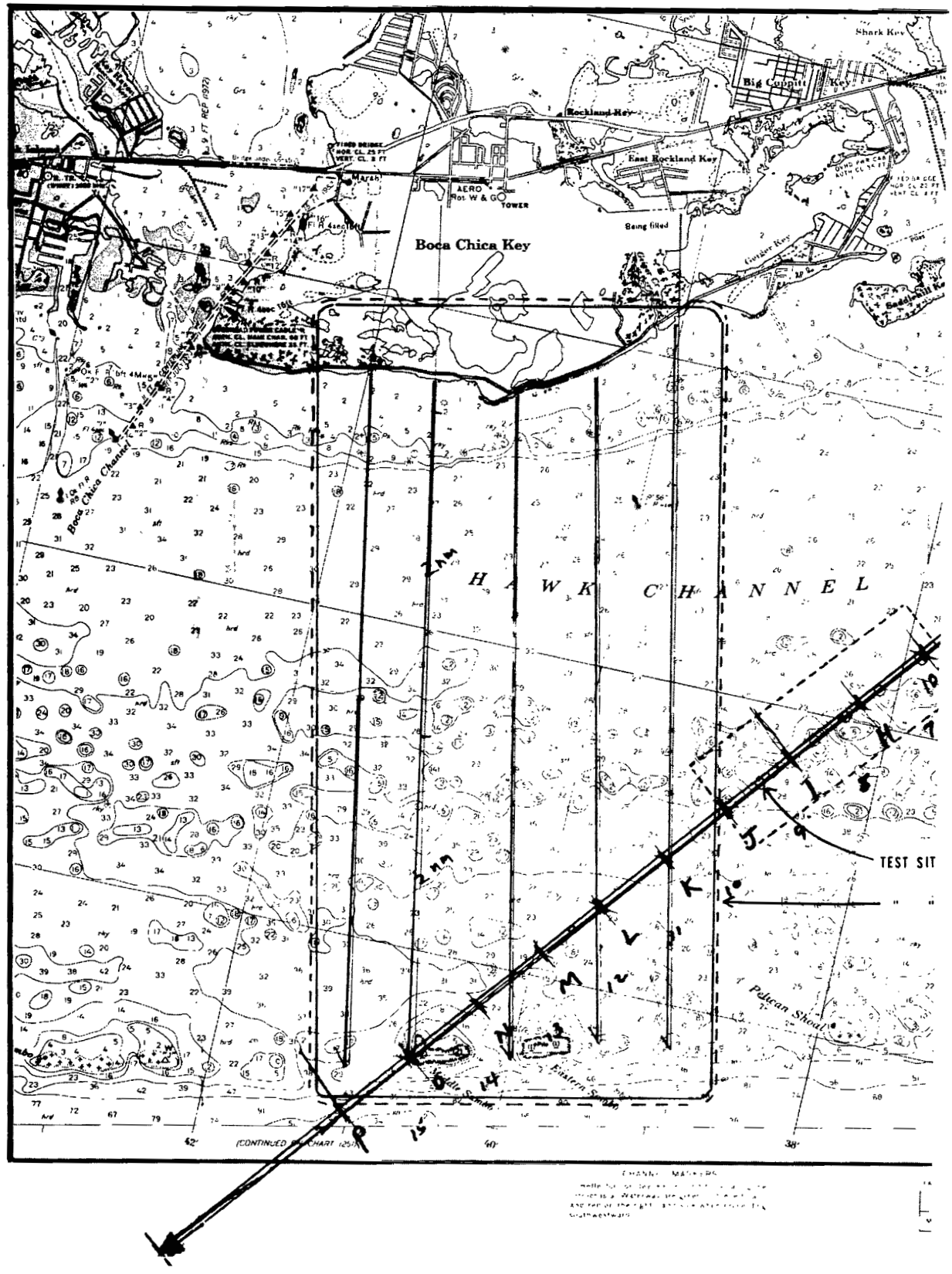

Figure 8. - Hydro chart of Boca Chica Area.

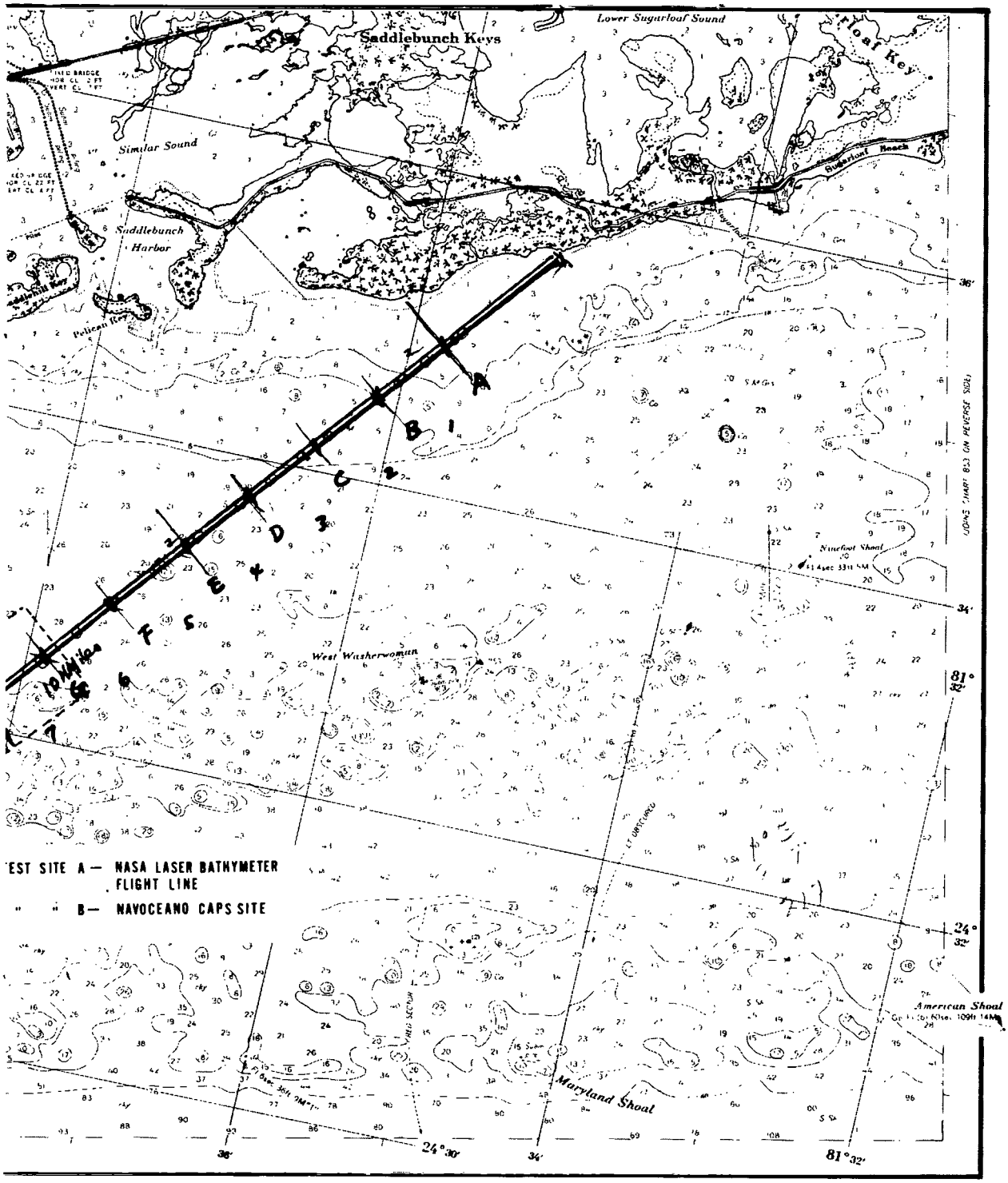

Figure 8. - (continued)

In both the August and February tests, a number of buoys were laid along the 15 km long flight path, subdividing the stretch into 17 zones as shown in the map. The sediments along the line were almost entirely carbonate and varied from a relatively coarse sand over most of the line to a very fine clay-silt in Hawk Channel (Zones C to G).

The vegetation occurs thickest in shoaly areas flanking the channels. From both sea and air the abruptness of these thick patches was noted, and as might be expected, these corresponded to diminished and often hard to interpret laser returns. Between these thick patches are fairly evenly spaced assemblages of grasses, small corals and sponges. The sponges often attained heights of 2 meters and are suspected to have interfered with some laser returns. (See fig. 9.)

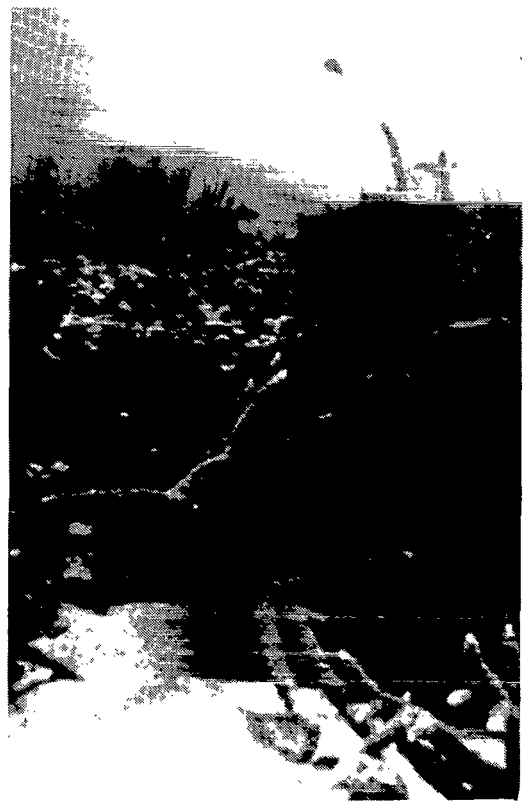

Figure 9. - Underwater vegetation.

In August 1974, 28 test runs in seven days were made in the area. In February 1975, 19 additional test runs were made in the same area. The complete test schedules, the data acquisition modes and experimental set up and purposes are listed in table II.

TABLE II. - KEY WEST FLIGHT TEST SCHEDULE

NEON LASER BATHYMETER FLIGHT TEST
(KEY WEST TEST AUG. 20-28, 1974)

DATE	FLT	RUN	TIME START	STOP	TOTAL RUN TIME	RUN LOCATION	HEADING	EXPERIMENT	SEA TRUTH	NOTE	FOOT PRINT CAMERA FRAME
8-20-74	1	1	17:05:00	17:06:50	1:50 sec	A	40°	Bathymetric	Buoy Markers	False Triggering	232-16-43:45 45:56
		2	17:17:25	17:19:20	1:55 sec	A	40°	"	Installed	" "	
		3	17:30:05	17:32:00	1:55 sec	A	40°	"		" "	
		4	17:43:20	17:45:10	1:50 sec	A	40°	"		Runs out film	
8-21-74	2	5	19:20:00	19:21:40	1:40 sec	A	40°	"	α-Measurements	Dusk Condition	
		6	19:28:00	19:30:00	2:00 sec	A	40°	"	B1, B3, B4, B2,	Oscilloscopic	233-19-10:17
		7	19:38:00	19:40:00	2:00 sec	A	40°	"	C55	Traces Recorded	
		8	19:48:00	19:49:50	1:50 sec	A	40°	"		in film	
8-22-74	3	9	17:49:10	17:49:50	0:40 sec	A (drift)	220°	"		Drifted off course	
		10	17:56:00	17:58:50	2:50 sec	A(extended to	220°	"		aborted good return	
		11	18:06:00	18:08:53	2:53 sec	M. Sambo)	220°	Polarizer			234:18:06:19 09:04
		12	18:16:13	18:19:06	2:53 sec	"	220°	Parallel			
		13	18:27:00	18:28:15	1:15 sec	"	220°	Cross		Runs out film	
8-23-74	4	14	16:33:00	16:35:55	2:55 sec	"	220°	No Polarizer			
		15	16:43:30	16:46:30	3:00 sec	"	220°	45° + N.D.#2			235:16:43:39 46:26
		16	16:55:00	16:58:03	3:03 sec	"	220°	45° + N.D.#1			
		17	17:07:17	17:09:15	2:58 sec	"	220°	Spatial Filter			
8-26-74	5		(High Altitude Rayleigh Scattering Measurements)								
	6	18	11:39:00	11:42:16	3:16 sec	"	220°	Open	α-Measurements		
		19	11:50:05	11:52:55	2:50 sec	"	220°	150/1000	B12, 6, 5, e-55, 4.13, 16, 15, 14, 12, 7, 6, C-55, B15		
8-27-74	7	20	16:54:00	16:55:30	1:30 sec	Wrong Course	160°	Mapping Exercise		Navoceano Test Site B	
		21	17:08:00	17:09:42	1:42 sec	B #2	160°	Mapping Exercise			239:16:50 16:52:00
		22	17:16:00	17:17:43	1:43 sec	B #3	160°	Mapping Exercise			239:17:08 17:10
		23	17:25:05	17:26:53	1:48 sec	B #4	160°	Mapping Exercise			
		24	17:32:40	17:34:00	2:00 sec	B #5	160°	Mapping Exercise			
		25	17:39:30	17:41:17	1:47 sec	B #1	160°	Mapping Exercise			
8-28-74	8	26	10:21:10	10:25:10	4:00 sec	A (Extended	220°	Bathymetric			240-10-21:00
		27	10:27:00	10:30:55	3:55 sec	beyond M.	40°	"			
		28	10:34:30	10:37:00	2:30 sec	Sambo)	220°	"		Runs out film	

FREQUENCY DOUBLED ND YAG LASER FLIGHT TEST
(KEY WEST TEST FEB. 19-27, 1975)

DATE	FLT	RUN	TIME START	STOP	ALTITUDE	RUN LOCATION	EXPERIMENT	DATA MODE	FOOT PRINT CAMERA
2-19-75	9	29	11:29:46	11:33:11	150 meters	A	OMA Real Time Instrumentation	OMA	11:29:46-11:33:11
		30	11:40:50	11:44:13	"	A	4X Film Test	Camera	
2-20-75	10		15:52:20	15:54:35	2000 meters	B	Zeiss Camera Test Run	(No laser data)	
			15:58:40	16:00:15	"	B	Zeiss Camera Test Run		
		31	16:03:35	16:07:12	600 meters	A	600 meter altitude run	(4X Film)	16:03:36-07:11 (159 images)
		32	16:15:01	16:18:25	600 meters	A	Repeat of Run #32	(Jittery Noise)	(150 images)
		33	16:26:10	16:29:37	150 meters	A	Repeat of Run #32 at lower altitude		
2-21-75	11	34	10:22:52	10:26:13	150 meters	A	Cross Polarization	(4X Film)	5 frame/sec (450 images)
		35	10:34:26	10:37:46	"	A	Parallel Polarization	"	no film images
		36	10:46:41	10:50:04	600 meters	A	600 meters altitude	"	0.75 frames/sec
		cancelled			600 meters				
2-24-75	12	Photo laser combination test postponed, instead photo calibration runs in AM due to extreme turbid water conditions							
2-25-75	13	Morning flight postponed							
		37	16:15:40	16:19:00	600 meters	A	OMA, A-B Mode Cross Polarization Test	OMA (R-003)	
							Test		
		Other runs postponed							
		Other runs postponed							
2-26-75	14	Bad weather and turbid water in the Key West test area and a new test site in the vicinity of Tortuga Island was searched							
2-27-75	15		08:59:30	Aborted	Off Course	A	OMA and Auto Tape Nav. System Test	(OMA AR-004)	
		38	09:06:08	09:09:37	600 meters	A	4X - Film Auto-Tape	(4X Film)	
		39	09:16:29	09:20:12	600 meters	A	OMA Real Time		
		40	09:50:12	09:52:43	600 meters	B	Stereo Photo-Laser Combination Test	(f-8, 1/400 sec. - camera)	
								and (OMA)	
	16	41	16:25:03	16:27:30	600 meters	B	Photo-Laser Combination Test	Mapping Exercise (OMA-Zeiss Camera)	
		42	16:30:51	16:35:30	"	B	"	"	
		43	16:42:49	16:45:13	"	B	"	"	
		44	16:50:52	16:53:16	"	B	"	"	
		45	16:59:21	17:01:37	"	B	"	"	
		46	17:14:05	17:16:26	"	B	"	"	
		47	17:25:37	17:29:13	"	A	"	"	

During the 20 day mission, about 120,000 laser shots were fired; 100,000 of the shots are recorded on 4X-film and 20,000 are recorded on 9-track tape, via the waveform digitizer.

For the most part, areas were surveyed by the surface vessel crew for the time flights had been planned. Since the flight altitudes did not exceed 600 meters, the cloud cover did not interfere in most of the flights. But for three days between February 24 to 26, the scheduled photo-laser combination tests were interfered by extreme turbid water at the test site as an aftermath of a mild tropical storm which passed through the islands the evening of February 22.

Whenever a test flight run was considered to be meaningful, the footprint camera on board was switched on in order to record the exact flight path and its underwater features. Excellent aerial coverage of the entire stretch is available from the altitudes of 150 meters and 600 meters. The enlarged aerial photo of Zones G to J is shown in figure 10. The images are from Run 34.

Ocean Floor Profile from the Field Data

The primary objective of the Key West test series was to evaluate the ALB technology in field conditions. The emphasis was on the studies of laser penetration capability, the effects of varying hydrospheric parameters on the operation, and instrumental performance. Therefore, the major portion of the data was recorded for this purpose. However, some of the return data could be used for creating a bottom contour of the test site. The underwater topographic contour shown in figures 10, 11, and 12 were all produced manually by point plotting the return waveforms of the 4X-film. Figure 10 pertains to more detailed underwater features of Zones G to J. The top aerial images are from the 35mm footprint camera, and dotted ocean floor contours were made from the results of Runs 34 and 36. The bottom bathymetric isobar chart was generated by combining the photo image information (through a stereo viewer) and the transecting laser data lines as reference. Figure 11 shows the laser data and corresponding sonar readout; figure 12 was generated in support of Navoceano's Coastal Area Photo Survey (CAPS) exercise (Test Area B on the map).

Computer Aided Data

As shown in the test schedule of table II, the significant effort was put in testing the waveform digitizer. This form of data gathering is essential in order to achieve a successful linkage to a computer. We were finally able to record the returns of Run 39 on tape on the afternoon of February 27. The remaining runs up to 41 were recorded on 9 track

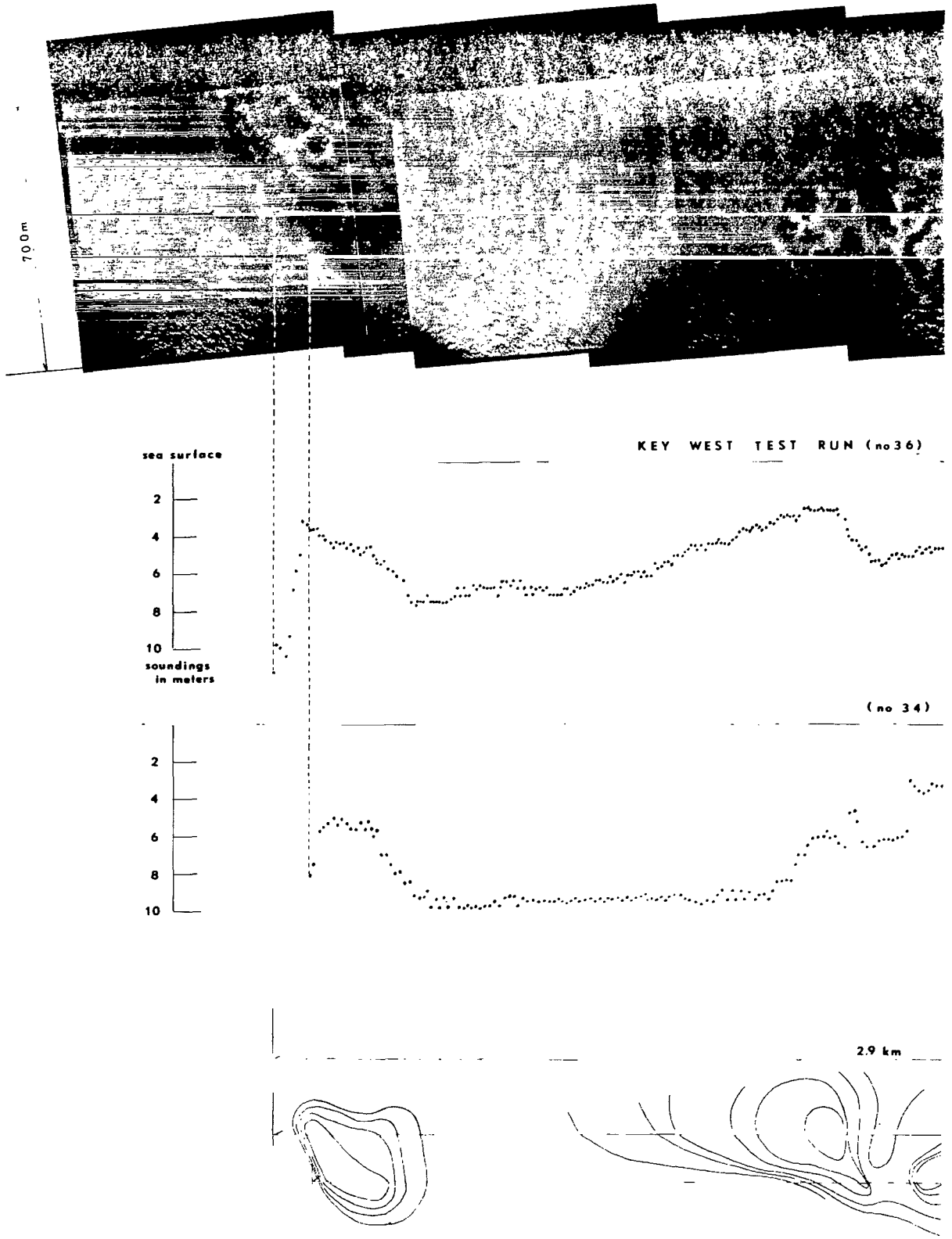

Figure 10. - Aerial photo coverage of Zones H to K.

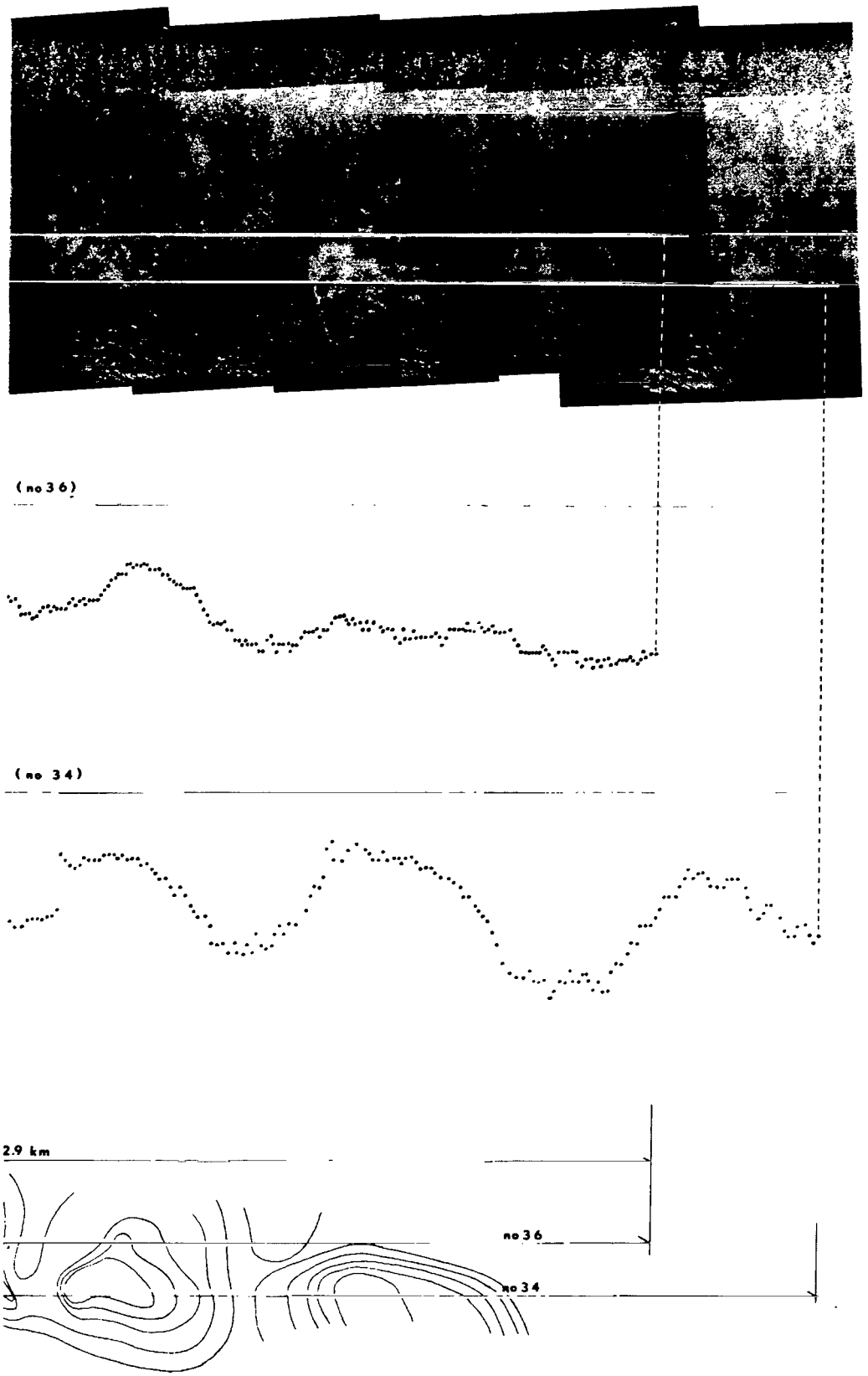

Figure 10. - (continued)

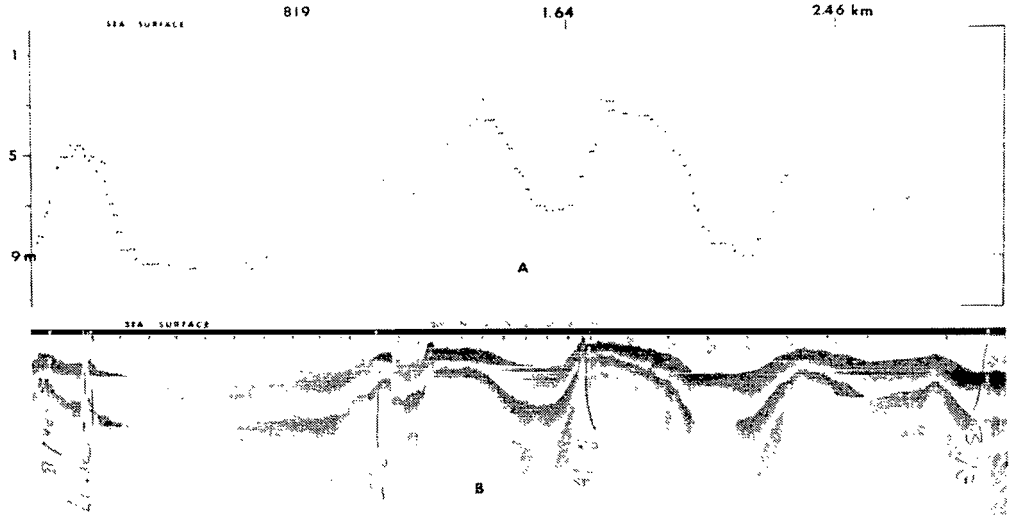

Figure 11. - Laser bathymeter bottom profile and matching sonar chart.

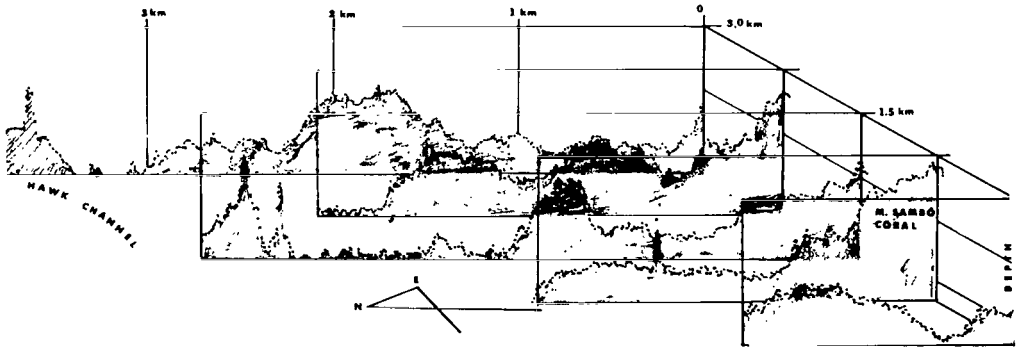

Figure 12. - Underwater topography created by an airborne laser bathymeter (CAPS Site).

magnetic tapes. It is unfortunate that the instrumentation does not afford the simultaneous recording of the return shots in both movie camera and a waveform digitizer. However, from the rolls of 9-track tape, we were able to process and display the flight results of Run 39.

The computer link, which was developed to process Run 39 data, is shown in figure 13 block diagram. An OMA on board transferred each transient pulse shape into 500 digital channels and each channel contained 2^8 bits of amplitude information. The digitizer is capable of handling such scans at the rate of 30 cycles per second. A software package was developed to process the waveform data on the Wallops Honeywell 625 computer. The main code transcribes the raw data into a form which is suitable for easy access and manipulation. One can then call a number of programs for further processing. Options include numerical printouts or continuous plots of the scans. A sample Calcomp plot of a waveform is shown in figure 7.

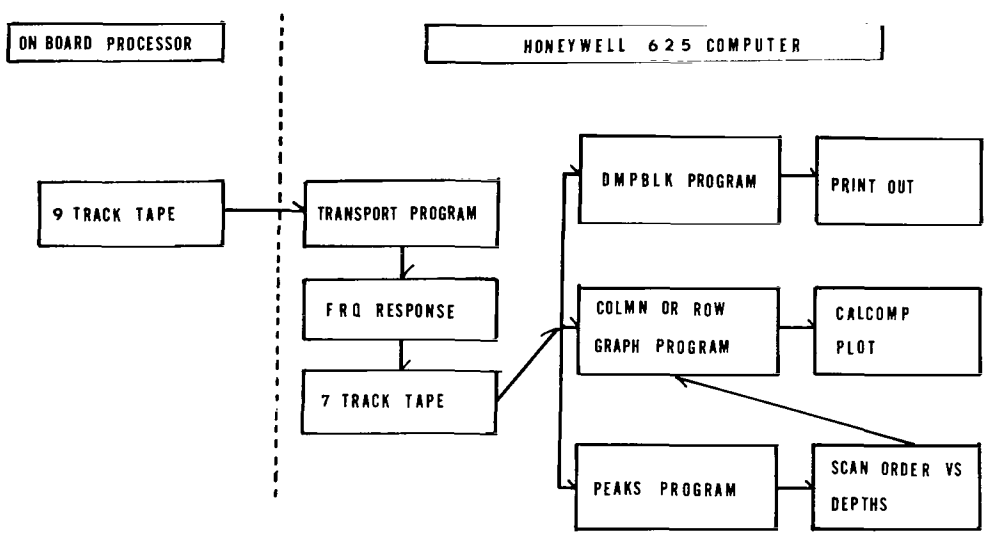

Figure 13. - Block diagram of computer linkage.

A program was also written to recognize the two highest peaks of a trace, and to transform the channel separation between the peaks into a depth reading. Data originating from Run 39 is shown in figure 14. Different rows pertain to consecutive laser returns. For instance, the waveform shown in figure 7 is taken from the 150th pulse of the Run 39 in the figure 14. The waveform shows the first intensity maximum in the 318th channel and

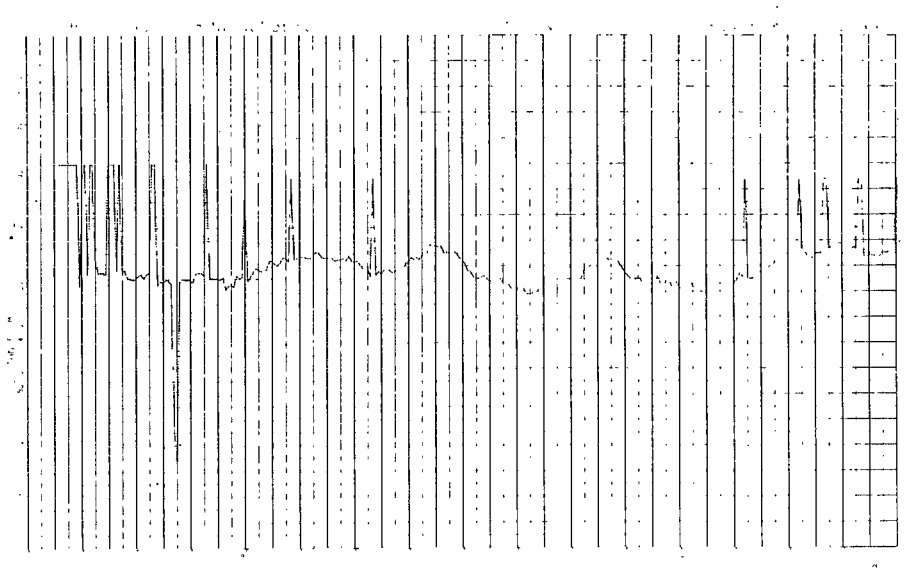

Figure 14. - Bottom profile by the computer output.

its amplitude was 600 counts whereas the second peak occurred in the 374th channel with relative amplitude count of 670. Fifty-six channels separate the two crests. This is equivalent to a photon transit time of 56 nanoseconds since the 500 channels represent 500 nanoseconds in this setting. Therefore, the corresponding depth at these points is about 6.27 meters and it is so registered in figure 14.

FURTHER ANALYSES OF SELECTED DATA

Table II summarizes all the NAS-427 test flights. Of the 47 flights, the results from the following four test runs were selected for further analysis. The reasons for selecting Runs 26, 34, 35, and 36 are:

a. Run 26 was made with a pulsed neon laser at the altitude of 150 meters.
b. Run 35 represents the returns from a Nd:YAG laser at the altitude of 150 meters.
c. Run 34 was the repeat of Run 35 except that the receiver had a linear polarizing filter normal to the incident beam polarization.
d. Run 36 was chosen as the run was essentially a repeat of Run 34 but at the altitude of 600 meters.

The 4X-film recordings of the return traces of all the four runs were excellent and coordinated sea-truth is available on both flight dates.

In the analysis, only those returns from Zones G to K of the test area were selected. The first and second peak amplitudes and their separation were entered. The chosen sample Zones G to K largely consist of rapidly changing bottom contours of mixed sand, coral and vegetation textures as shown in figure 9 (underwater scene). The water clarity of the area was relatively uniform. Each run yielded about 200 data points in each category.

Surface Reflectance

Time averaged reflectance at normal incidence from a smooth sea surface is nominally 2% from the relation

$$R = \frac{E(r)^2}{E(i)^2} = \left(\frac{n-1}{n+1}\right)^2 = 0.02 \qquad (11)$$

where E(i) and E(r) denote the amplitudes of the electric vectors in the incident and reflected. In pulsed operation, the reflectance varies from pulse to pulse and the characteristics of the reflected and transmitted beams depend on the angle of incidence of the beam on the local wave slopes. A slope-frequency function represents a time average distribution of slopes at a point on the ocean surface and it can be developed to express a time average reflection.

Table III was tabulated for the analysis of laser beam reflection. The third column of the table denotes the mean averaged values of the surface reflection peaks of each run.* Unfortunately the scale is arbitrary, only the mean values of Runs 34 and 35 are relative. However, it shows that our mean averaged figures are comparable to the nominal 2% surface reflectance.

---

* Definition of sample average (Mean Average) and the sample variance (S.D.)

$$\bar{y} = \frac{1}{n}\sum_{k=1}^{n} y(x_k) \qquad \bar{y} = \text{a function } y(x) \text{ of the random variable } x$$

$$s^2 = \frac{1}{n}\sum_{k=1}^{n} (x_k - \bar{x})^2 \qquad s = \text{standard deviation is a measure of dispersion of the sample distribution}$$

TABLE III. - MEAN AVERAGED SEA SURFACE REFLECTION PEAKS AND ITS STANDARD DEVIATIONS

	Data Pts.	Surface Reflection Mean Average	Std. Deviation	S.D./M.A.
Run #26	187	1.956	0.302	.15
Run #34	205	1.187	0.618	.52
Run #35	213	4.295	0.633	.15
Run #36	281	2.030	0.700	.34

The table also shows the tendency of increasing standard deviations for cross polarized reflections as in Runs 34 and 36 in comparison with Runs 26 and 35. More direct comparison of polarization analysis of the surface return can be seen by comparing Runs 34 and 35 as given in table IV and its histogram in figures 15. Both runs were made at the altitude of 150 meters and the laser beam spot size on the sea surface was about 50 cm in diameter. Moderate 4 to 5 knot winds prevailed on the morning and bright tropical midmorning sun and clear water were the flight conditions. The Nd:YAG laser beam was totally polarized as the output was in the cavity dumping mode by the polarization coupling technique. Therefore, by simply changing the direction of the receiver polarizer, the surface reflectances via the reflection polarized normal to the direction of the plane of incidence (Run 34) and the reflection polarized parallel (Run 35) can be compared. A wide fluctuation in the amplitude was expected as the random distribution of the resolved sea slopes by the narrow laser beam will result in random reflectivity. One would expect that the wind conditions or sea surface roughness would directly influence the skewness of the distribution. At any rate, the mean averaged amplitude of Run 34 is smaller than Run 35 by a factor of almost four. This means that the surface is about a 25% efficient isotropic depolarizing scatterer, if we define a 50-50 intensity ratio as 100% depolarization. This surprisingly large depolarization effect in relatively calm waters should be interpreted as favorable to the design of a scanning airborne lidar system; the isotropic reflection of 0.5% from off normal incidence is not expected to drop off very sharply as the angle of incidence increases. Thus one would always expect consistently recognizable surface returns at any scan angle.

TABLE IV. - SURFACE REFLECTION PULSE HEIGHT DISTRIBUTION

Pulse Amplitude	Data Points From Run 34	Data Points From Run 35
0.2	1	
0.4	13	
0.6	25	
0.8	30	
1.0	31	
1.2	21	
1.4	24	
1.6	11	
1.8	10	
2.0	8	
2.2	4	
2.4	4	
2.6	2	
2.8	2	
3.0	1	
3.2	-	-
3.4		1
3.6		11
3.8		12
4.0		21
4.2		25
4.4		27
4.6		40
4.8		28
5.0		25
5.2		13
5.4		6
5.6		1
5.8		0
6.0		2
Total Data Points Entered	187	212

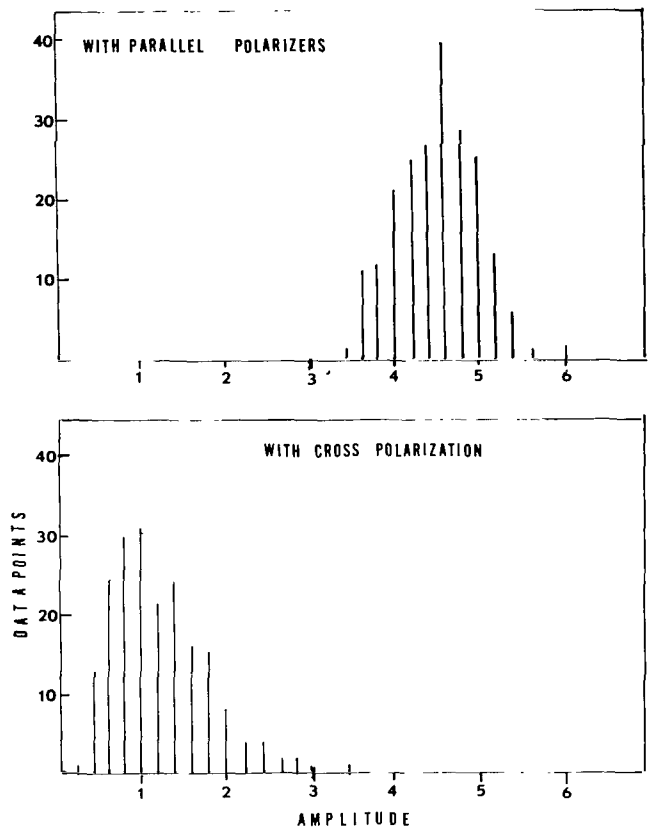

Figure 15. - Histograms from surface reflection data.

Effective Attenuation Coefficient

In table V the return amplitudes of each run from various bottom depths are listed along with their standard deviations. The peak distribution was random as in the surface reflections and a fairly constant ratio of the standard deviation to the mean averaged amplitude is observed. The comparison of Runs 34 and 35 shows that the average peak heights are in the ratio of 6 to 4. One could infer from this observation that the sea bottom in the area is about a 66% effective depolarizer or randomizer of the polarized beam.

TABLE V. - MEAN AVERAGED BOTTOM REFLECTION PEAKS

Depths (in meters)	Run #26		Run #34		Run #35		Run #36	
	Mean Avg	Std Dev	Mean Avg	Std Dev	Mean Avg	Std Dev	Mean Avg	Std Dev
3.13	1.102	0.188	2.452	0.512	3.30	0.389	2.471	0.362
3.58	0.937	0.120	2.226	0.480	2.940	0.499	2.287	0.550
4.02	0.930	0.115	1.731	0.467	2.638	0.474	1.872	0.511
4.47	0.875	0.170	1.233	0.476	2.200	0.358	1.449	0.367
4.92	0.886	0.135	1.000	0.346	1.925	0.409	1.307	0.403
5.36	0.700	0.128	0.876	0.385	1.744	0.430	1.014	0.366
5.81	0.705	0.148	0.880	0.241	1.428	0.319	1.205	0.302
6.26	0.640	0.164	0.789	0.220	1.090	0.401	0.984	0.284
6.71	0.454	0.157	0.638	0.274	0.930	0.134	0.707	0.126
7.17	0.440	0.105	0.470	0.133	0.956	0.274	0.681	0.105
7.60	0.500	0.284	0.400	0.141	0.650	0.135	0.578	0.092
8.05	0.350	0.164	0.366	0.072	0.540	0.171	0.577	0.086
8.49	0.262	0.103	0.358	0.073	0.380	0.147	0.489	0.083
8.94	0.174	0.066	0.246	0.079	0.294	0.103	0.424	0.092
9.39			0.205	0.073	0.224	0.070	0.344	0.070
Total Data Points Entered		204		205		213		271

Tabulated amplitudes from table V can be used for the calculation of the effective attenuation coefficients of the ALB unit. For we know, the empirically tabulated return signal intensity is a function of the optical path length. We can calculate the effective attenuation constant, γ, from the following relation:

$$I(L') = I(L)e^{-2\gamma (L'-L)} \tag{12}$$

where, I(L) denotes the observed mean intensity at the water depth of point, L, as received by the NASA ALB unit. The results of the γ calculations are listed in table VI and the results of Runs 35 and 36 are plotted in figure 16. The empirical data shows that the actual laser beam is only attenuated at the rate of exponential 0.2 m^{-1} as the beam is propagated downward and returned to the surface.

TABLE VI. - EFFECTIVE ATTENUATION COEFFICIENTS AS THE FUNCTION OF DEPTHS

L' – L (in m)	γ (m^{-1}) #34	#35	#36
8.0 - 4.5	0.194	0.109	
8.9 - 5.36	0.256	0.133	0.153
9.8 - 6.26	0.250	0.136	0.156
10.7 - 7.15	0.230	0.142	0.199
11.6 - 8.05	0.205	0.161	0.143
12.5 - 8.94	0.175	0.197	0.143
13.4 - 9.83	0.147	0.192	0.160
14.3 - 10.7	0.168	0.157	0.45
15.2 - 11.6	0.175	0.220	0.125
16.1 - 12.5	0.196	0.217	0.164
16.9 - 13.4	0.176	0.235	0.156
17.8 - 14.3	0.213	0.257	0.142
18.7 - 15.2	0.185	0.324	0.152
Avg.	0.187	0.203	0.153

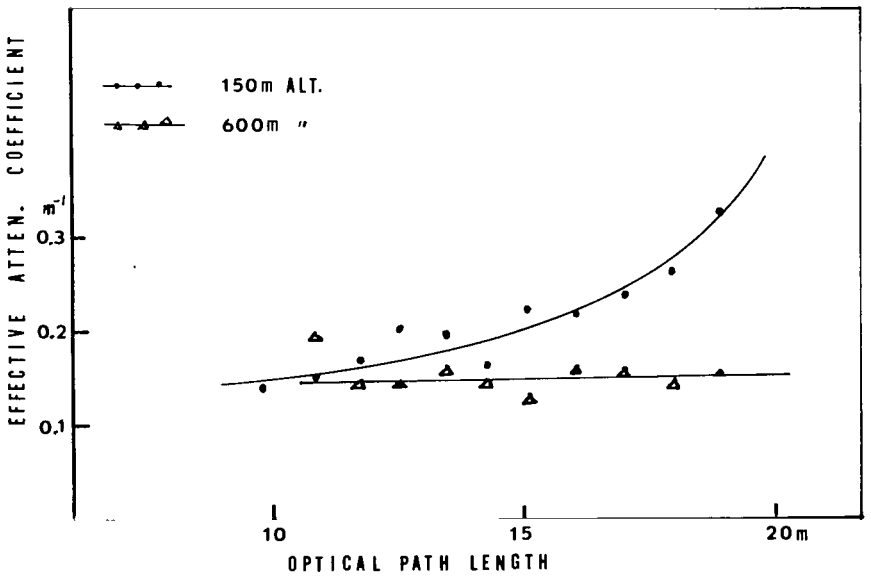

Figure 16. - γs from runs 35 and 36.

For reference, the in situ measurements of alpha values at the approximate time of the flights are given in table VII and figure 17.* The buoy marks, 7, 13, 20, and 18, denote the boundaries of Zones G, H, I, and J on the map (figure 17). From the data, we see that the averaged alpha values are five times larger than the gamma and this ratio is expected to be variable depending on the transmitter/receiver geometry and volume scattering function of the sea water medium. This can be shown by comparing the gamma values from Runs 35 and 36 as shown in figure 16. At the platform altitude of 150 meters, the field of view of the ALB receiver was not sufficiently large enough to contain all the forward scattering lobe of the upwelling light as the depth increases beyond 7 to 8 meters in Run 34. Therefore, increasing losses due to the receiver geometry have resulted in the upward tendency in the plot in figure 16, whereas the 600 meter altitude flight data indicates fairly uniform gamma values regardless of depth. This discrepancy between α and γ was observed earlier by Hickman[8] in his laboratory experiments. In these studies both quartz and natural sediment were used to mock-up the water turbidity conditions. An effective attenuation coefficient ($\alpha_{eff} = \beta \cdot \frac{a}{s}$) was defined by Hickman to explain the results of these experiments. In his expression, β = constant (3.30) while a and s are the absorption and scattering coefficients, respectively.

TABLE VII. - IN SITU α-READINGS

Sample Depth	Transmissivity Ave.	Alpha	Depth	Secchi Reading	Ave. Alpha	Ave. Alpha to Secchi
		Station 7 2-21-75				
-1	46.5	.78				
-2	40.5	.90				
-3	38.5	.96				
-4	36.5	1.02	7.0	4.95 (5)	.98	.94
-5	35	1.05				
-6	33.5	1.09				
-6 1/2	33	1.10				
		Station 13 2-21-75				
-1	40.5	.90				
-2	42	.88	4.3		.87	
-3	43	.85				
-4	43	.85				
		Station 19 2-21-75				
-1	46	.78				
-2	50	.71	3.8		.73	
-3	50	.71				
		Station 20 2-21-75				
-1	43	.85				
-2	43.5	.84				
-3	44	.83	7.8	5.1(5)	.83	.84
-4	44	.83				
-5	44	.83				
-6	44	.83				
-7	44	.83				

* The sea-truth data along the flight line was made available to us by R. N. Swift, Marine Science Consortium, Lewes, Delaware.

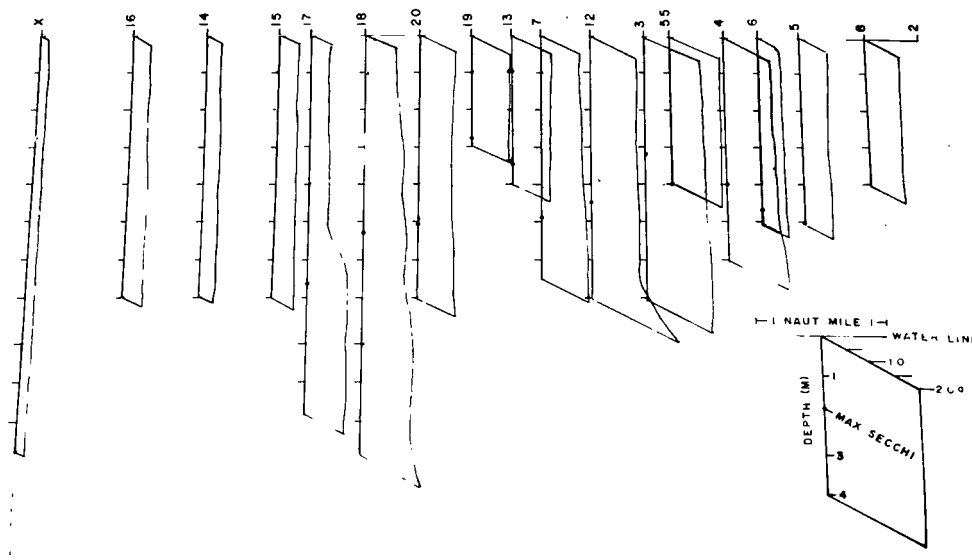

Figure 17. - α-readings along the survey line.

DISCUSSION AND CONCLUSIONS

In practice, the use of the ALB is limited to shallow coastal waters. This is due to the moderate losses experienced underwater by a light beam. The practical implementation of such a system raises a number of questions:

a. What is the maximum dynamic range attainable?
b. How can an ALB unit be actually used in mapping?
c. Is it possible to design an active scanning device to cover a wider lateral swath?

In order to clarify some of these questions, the limitations inherent to ALB technology are discussed in this section.

ALB performance is ultimately limited by noise. The background level has contributions from atmospheric light and sea surface modulation. When the ALB is flown in total darkness over smooth waters, the minimum detectable signal depends only on the shot noises in the photomultiplier tube. In daylight operation, however, the background dc level becomes several orders of magnitude larger and the background contributes a power

$$P(b) = \frac{S \cdot A_{(surf)} \cdot E \cdot T_{(f)} \; \Delta\lambda \cdot e^{-KH} \cdot d\Omega}{\frac{hc}{\lambda(\ell)}} \tag{13}$$

where S is the sea surface irradiance in watts/$\Delta\lambda$ - cm^2. This quantity depends on the incident sun angle, sea surface reflectivity, etc. The receiver sees an area, A (surf), on the sea surface. A spectral filter with transmittance, T(f), and a frequency window, $\Delta\lambda$, is used to reduce the effect of sunlight.

If P_o is the laser power received, then against the background, P(b), the system can resolve a maximum depth

$$L \text{ max} = \frac{\ell n \sqrt{\frac{P_o}{P(b)}}}{\gamma} \tag{14}$$

and γ is the effective attenuation coefficient as measured by the ALB.

Figure 18 is a plot of equation 14. The maximum depth is shown as a function of γ for varying values of $P_o/P(b)$. We estimate that this ratio can be as large as 10^7 at night. This value is derived on the assumption that a photomultiplier tube is operating under a noise requirement power of 10^{-10} W with a 50 ohm termination in total darkness and a frequency doubled Nd:YAG laser of 2 MW peak power being flown at 600 meters. With a value of γ = .175 m^{-1} typical of the Key West waters, the maximum depth is 50 meters. In daylight operation, the ratio of $P_o/P(b)$ varies from 10 to 10,000 (at dusk). The plots in figure 18 are valid for any ALB system. It is interesting to note that P_o, P(b) and γ are all quantities that can be measured from an airplane platform. A well designed ALB comprising a minicomputer, under favorable weather and turbidity conditions, could be able to predict the performance of the system for the mission.

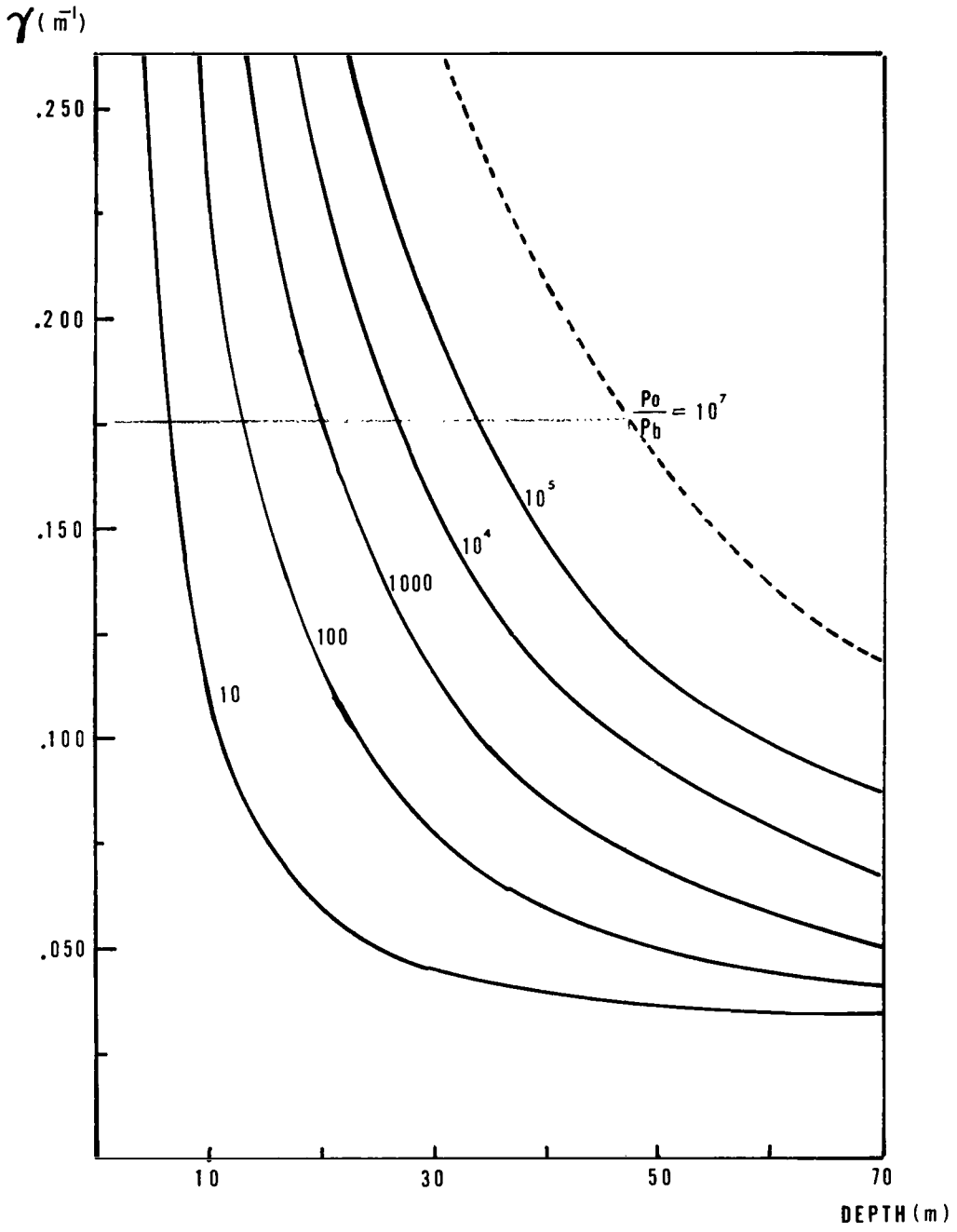

Figure 18. - Maximum depth range.

APPENDIX A

AGREEMENT BETWEEN THE U.S. NAVAL OCEANOGRAPHIC OFFICE, HYDROGRAPHIC DEVELOPMENT DIVISION AND NASA WALLOPS STATION ON THE DEVELOPMENT OF AN AIRBORNE LASER DEPTH SOUNDING SYSTEM

1. BACKGROUND

a. The U. S. Naval Oceanographic Office (NAVOCEANO) has a continuing requirement to conduct hydrographic surveys along coastlines throughout the world. During the period from 1967 through 1970 NAVOCEANO developed and flight tested a Pulsed Light Airborne Depth Sounder (PLADS). These tests, in an H-3 helicopter, demonstrated the capability to measure water depths with accuracy and proved the feasibility of airborne depth sounding at speeds in excess of 50 knots. This breadboard PLADS system was tested well beyond its expected operating life and, due to funding limitations, testing was discontinued before specifications for an Advanced Development Model (ADM) could be developed. Also, the equipment did not provide the desired digital output on magnetic tape. Because of NASA's efforts with various LIDAR systems it was decided to combine our resources and technical expertise for further development of a laser depth sounder.

b. NASA Wallops Station under the funding of the NASA-OAST Office has been engaged in the research and development of an airborne hydrographic LIDAR system. In its two years of existence the program has produced the first helicopter-borne laser chlorophyll-A fluorosensor (1972) and an airborne laser oil fluorosensor in 1973. In fiscal year 1974, the program will focus its activities on the problems of developing a prototype pulsed laser bathymeter which can be flight tested and used to develop specifications for an ADM capable of being used by NAVOCEANO to conduct nearshore hydrographic surveys to at least the five fathom curve in most coastal areas.

c. Meetings between NASA and NAVOCEANO personnel during the past two months have produced this mutual agreement on objectives and approach in the development of an improved airborne laser depth sounder.

2. WORK STATEMENT

a. NASA will develop and test signal processing equipment to provide the water depth information in digital form on magnetic tape. The development objectives for this time to digital signal processing unit are:

(1) Time accuracy: 1 nanosecond or better
(2) Reliability: 2,000 hours MTBF or better
(3) Weight: 20 kilograms or less
(4) No serious packaging problems
(5) Design criteria for estimated production costs of $15,000 or less

b. NASA will investigate new techniques, such as mode locked pulse, for generating shorter and more powerful optical pulses for the laser transmitter. For this purpose, NAVOCEANO will loan the existing PLADS system to NASA.

c. The feasibility of using a time gating technique to enhance the signal to noise ratio of the bottom reflection pulse will be studied.

d. Throughout this effort, NASA will evaluate design criteria, such as optimum polarization of transmitted beam, spatial and spectral filtering of the receiver optics, radiation safety, ease of operation, etc., useful for future operational system development. NASA will use both PLADS and the existing NASA LIDAR systems for this objective.

e. NASA will provide quarterly reports to NAVOCEANO during the time period of this effort. These reports will include all results, developments, data, etc., that may be of use to NAVOCEANO to improve the design criteria for an operational prototype laser depth sounder. A Purchase Description for the PLADS is provided with this work statement as an example of the type of information needed. This Purchase Description was used to purchase the PLADS in 1968 and does not reflect today's state-of-the-art. Two NAVOCEANO Technical Notes, Numbers 6620-102-72 and 6200-1-72 are also provided. These two reports cover development and test of the PLADS and will be used by NAVOCEANO in the development of new performance specifications.

3. SCHEDULE

a. This joint development program will be carried out in two phases. Phase I will include:

(1) Development of a Signal Processing Unit
(2) Flight tests of the NASA laser and receiver
(3) Shipment of PLADS equipment to NASA-Wallops
(4) Investigation of new pulse compression techniques
(5) Investigation of gating technique applicability

b. Initiation of Phase II will be dependent on the mutual agreement of NASA and NAVOCEANO at some future date. Phase II will include:

(1) Flight test of the signal processing unit with the complete system
(2) Analysis of test data
(3) Development of performance specifications for an Advanced Development Model (ADM)
(4) Preparation of final report.

APPENDIX B

UNDERWATER PROPAGATION MODEL

An expression in closed form can be derived for the monochromatic light power transmitted between a circular spot, As, of radius, Rs, at the bottom of the water and a circular surface, Ac, of radius, Rc, at the sea-air interface. We consider the bottom surface, As, to be uniformly illuminated and call the power density, W (see figure).

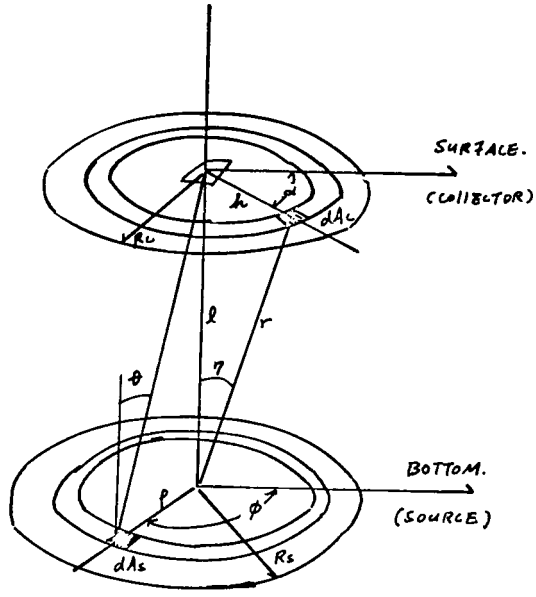

Figure B-1. - Geometry of laser beam underwater propagation.

1. For an element of area, dAc, on axis receiver from an element of area at the bottom, dAs, the power can be expressed as:

$$d^2P_{s\to c} = \left(\frac{W \cdot dAs \cos\theta}{\pi r^2} \right) dAc \cos\theta \qquad (B1)$$

where the first cosine is due to Lambert's law and

$$\cos\theta = \frac{\ell}{r} \; ; \quad dAs = \rho d\rho d\phi \qquad (B2)$$

substituting

$$d^2P_{s\to c} = \frac{W\ \rho d\rho d\phi \cdot \ell^2\ dAc}{\pi(\ell^2 + \rho^2)^2} . \tag{B3}$$

Integrating over the source variables we get

$$dP_{s\to c} = dAc\ \frac{W}{\pi}\ \frac{\ell^2}{2} \int_{\rho=0}^{Rs} \frac{d(\ell^2 + \rho^2)}{(\ell^2 + \rho^2)^2} \int_{\phi=0}^{2\pi} d\phi$$

$$= dAc\ \frac{P_o}{\pi(\ell^2 + R_s^2)} \tag{B4}$$

where P_o is the total power radiated by As.

2. The total power received at the collector can be calculated by making either of two assumptions and we shall show the results to be equivalent.

a. First approximation

We assume that the power received by a small off-axis element, dAc, of collector area is approximately equal to

$$dP_{s\to c} = dP_{s\to c}\ (\text{on-axis})\ \cos\eta \quad \text{where } \cos\eta = \frac{\ell}{r} \tag{B5}$$

$$dP_{s\to c} = dAc\ \ W \left\{ 1 - \frac{\ell^2}{\ell^2 + R_s^2} \right\} \ \frac{\ell}{r}$$

$$= hdh\ d\alpha W \ \left\{ 1 - \frac{\ell^2}{\ell^2 + R_s^2} \right\} \ \frac{\ell}{[h^2 + +\ell^2]^{1/2}} . \tag{B6}$$

Integrating

$$P_{s\to c} = \int_{\alpha=0}^{2\pi} \int_{h=0}^{Rc} d\alpha \cdot W \cdot \ell \left\{ 1 - \frac{\ell^2}{\ell^2 + R_s^2} \right\} \frac{1}{2} \ \frac{d(h^2 + \ell^2)}{\sqrt{h^2 + \ell^2}}$$

$$= \frac{2W\ (\pi R_s^2)}{R_s^2} \ \ell \left\{ 1 - \frac{\ell^2}{\ell^2 + R_s^2} \right\} \ \left\{ \sqrt{R_c^2 + \ell^2} - \ell \right\} \tag{B7}$$

then

$$P_{s\to c} = P_s \left\{\frac{2\ell}{\ell^2 + R_s^2}\right\} \left\{\sqrt{R_s^2 + \ell^2} - \ell\right\}. \tag{B8}$$

(In terms of the total power, Ps, at the source.)

b. Alternately one can also approximate the power seen by an off-axis area element as:

$$P_{s\to c} = \int dAc\ W \left\{1 - \frac{\ell^2}{\ell^2 + R_s^2 \cos^2 \eta}\right\}$$

$$= \int_{h=0}^{R_c} \int_{\alpha=0}^{2\pi} hdh\ d\alpha \cdot W \cdot \left\{1 - \frac{\ell^2}{\ell^2 + \frac{R_s^2 \ell^2}{h^2 + \ell^2}}\right\}$$

$$= W\pi R_s^2\ \ell n \left(\frac{R_c^2 + R_s^2 + \ell^2}{\ell^2 + R_s^2}\right)$$

$$= W(\pi R_s^2)\ \ell n \left\{1 + \frac{R_c^2}{\ell^2 + R_s^2}\right\}. \tag{B9}$$

Then in terms of the total power, Ps, at the source

$$P_{s\to c} = Ps\ \ell n \left\{1 + \frac{R_c^2}{\ell^2 + R_s^2}\right\}. \tag{B10}$$

c. Equivalence of the two expressions, equations (B8) and (B10), Expression (B8) can be rewritten

$$P_{s\to c} = Ps \left\{\frac{2\ell}{\ell^2 + R_s^2}\right\} \left\{\sqrt{R_c^2 + \ell^2} - \ell\right\}$$

$$= Ps \left\{\frac{2\ell^2}{\ell^2 + R_s^2}\right\} \left\{\sqrt{1 + \frac{R_c^2}{\ell 2^2}} - \ell\right\}. \tag{B11}$$

Taking the first 2 terms in the series expansion of the square root we have:

$$P_{s\to c} \sim Ps \left\{ \frac{2\ell^2}{\ell^2 + R_s^2} \right\} \left\{ 1 + \frac{R_c^2}{2\ell^2} - 1 \right\}$$

$$\sim Ps \frac{R_c^2}{(\ell^2 + R_s^2)} . \qquad \text{(B12)}$$

Now we can also expand expression (B10) as

$$P_{s\to c} = Ps \ln \left\{ 1 + \frac{R_c^2}{\ell^2 + R_s^2} \right\}$$

$$P_{s\to c} \sim Ps \frac{R_c^2}{(\ell^2 + R_s^2)} \qquad \text{(B13)}$$

which is the same as (B12).

REFERENCES

1. Levis, C. A.; Swarner, W. G.; Prettyman, C.; and Reinhardt, G. W.: "An Optical Radar for Airborne Use Over Natural Waters", Hydrographic Lidar Conference Proc., NASA-SP-375, 1975.
2. Hickman, G. D. and Hogg, J. E.: "Application of an Airborne Pulsed Laser for Near Shore Bathymetric Measurements", Remote Sensing of Environment 1, Elsevier, NY, 1969, pp. 57-58.
3. Bright, D.: "Report on the Naval Oceanographic Office's Activity on Optical Depth Sounding Technique", Hydrographic Lidar Conference Proc., NASA-SP-375, 1975.
4. Duntley, S. Q.: "Light in the Sea", J.O.S.A., Vol. 53, pp. 221-224.
5. Hickman, G. D.; Hogg, J. E.; and Spadaro, A. R.: "Optical Attenuation Measurements of a Pulsed Neon Laser in Turbid Waters", SURC Technical Report (N00-24-69-C-1090), 1969.
6. Wells, W. H.: "Theory of Small Angle Scattering", AGARD-LS-61, NATO publication.
7. Kim, H. H. and Hickman, G. D.: "Airborne Laser Fluorosensor for the Detection of Oil on Water", ISA-JSP 6720, 1973, p. 369.
8. Hickman, G. D. and Ghovanlow, A. H.: "Preliminary Design Criteria, Performance and Limitations of an Airborne Laser Bathymetric System", Sparcom, Inc., Tech. Report No. IV, Contract N000-14-716-0202, August 1973.

"The aeronautical and space activities of the United States shall be conducted so as to contribute . . . to the expansion of human knowledge of phenomena in the atmosphere and space. The Administration shall provide for the widest practicable and appropriate dissemination of information concerning its activities and the results thereof."

—NATIONAL AERONAUTICS AND SPACE ACT OF 1958

NASA SCIENTIFIC AND TECHNICAL PUBLICATIONS

TECHNICAL REPORTS: Scientific and technical information considered important, complete, and a lasting contribution to existing knowledge.

TECHNICAL NOTES: Information less broad in scope but nevertheless of importance as a contribution to existing knowledge.

TECHNICAL MEMORANDUMS: Information receiving limited distribution because of preliminary data, security classification, or other reasons. Also includes conference proceedings with either limited or unlimited distribution.

CONTRACTOR REPORTS: Scientific and technical information generated under a NASA contract or grant and considered an important contribution to existing knowledge.

TECHNICAL TRANSLATIONS: Information published in a foreign language considered to merit NASA distribution in English.

SPECIAL PUBLICATIONS: Information derived from or of value to NASA activities. Publications include final reports of major projects, monographs, data compilations, handbooks, sourcebooks, and special bibliographies.

TECHNOLOGY UTILIZATION PUBLICATIONS: Information on technology used by NASA that may be of particular interest in commercial and other non-aerospace applications. Publications include Tech Briefs, Technology Utilization Reports and Technology Surveys.

Details on the availability of these publications may be obtained from:

SCIENTIFIC AND TECHNICAL INFORMATION OFFICE

NATIONAL AERONAUTICS AND SPACE ADMINISTRATION

Washington, D.C. 20546